World Journal of Engineering Research
Print ISSN: 2959-9865
Online ISSN: 2959-9873
DOI: https://doi.org/10.61784/wjer3080

SIMSCAPE-EQUIVALENT MODELING AND VERIFICATION OF A GAN DEVICE SPICE BEHAVIORAL MODEL FOR PV DC–DC SYSTEM-LEVEL SIMULATION

ZiYu Qin, Tu Hong, Lei Shi*
College of Automotive and Energy Engineering, Tongji University, Shanghai 201804, China.
**Corresponding Author: Lei Shi*

Abstract: A Simulink/Simscape-compatible device model is developed for system-level simulation of PV DC–DC power conversion, using a vendor-provided SPICE behavioral subcircuit of the EPC2302 GaN power transistor. After an automatic translation from the SPICE netlist to a Simscape description, semantic and syntactic incompatibilities are analyzed and are found to mainly originate from representing voltage-dependent capacitances as parameterized primitive components, which introduces runtime terminal voltages into parameter evaluation and leads to compilation conflicts. To preserve the device dynamic behavior while complying with Simscape semantics, the voltage-dependent capacitances are reformulated as explicit branch-current relations at the equation level, and the smooth fitting structure of the vendor model is retained to enhance numerical robustness. A datasheet-referenced verification workflow is established to assess consistency in static conduction behavior and dynamic capacitance-related characteristics. The resulting model compiles successfully and runs stably in time-domain simulations, providing a practical foundation for system-level transient analysis and loss-trend evaluation of high-frequency GaN DC–DC converters.
Keywords: Photovoltaics; DC-DC converter; Gallium nitride; Circuit simulation; SPICE; Nonlinear capacitance

1 INTRODUCTION

Against the backdrop of the carbon peaking and carbon neutrality goals and the continued growth in renewable energy installations, photovoltaic (PV) power generation systems are rapidly evolving toward higher efficiency, greater reliability, and higher power density [1]. In a typical grid-connected PV system, the wide-range DC voltage generated by PV modules or arrays must be converted and regulated to the voltage level required by the downstream DC bus or inverter, while maximum power point tracking (MPPT) must also be implemented to accommodate operating-point variations caused by changes in irradiance and temperature [2]. Therefore, the DC–DC converter serves as a critical energy conversion and control interface in PV power generation systems, and its performance directly affects the system's energy yield, volumetric and gravimetric characteristics, and levelized cost of electricity over the entire lifecycle [3].

As photovoltaic systems continue to pursue higher switching frequencies, greater power density, and higher efficiency, the adoption of wide-bandgap semiconductor devices has become a major trend [4]. Among these devices, gallium nitride (GaN) power devices are characterized by fast switching speed, low gate charge and output charge, and strong suitability for high-frequency operation [5]. These features make them promising for significantly reducing switching losses and shrinking passive component size in high-frequency DC–DC converters at low- and medium-voltage levels, thereby improving both power density and dynamic response [6]. In recent years, GaN devices have demonstrated considerable potential for enhancing efficiency and power density in photovoltaic module-level power electronics, such as optimizers and front-end stages of microinverters, as well as in grid-connected inverters [7-10]. At the same time, their high voltage slew rate (dv/dt) and strongly nonlinear terminal-equivalent capacitances impose more stringent requirements on circuit design, electromagnetic interference (EMI) control, and reliability [11]. In addition, panel-integrated DC–DC architectures and the associated performance trade-offs in PV-related applications have been systematically investigated, providing important guidance for realizing high-power-density designs [12-15].

In this context, accurate device-level models constitute an essential foundation for PV DC–DC topology design, control strategy verification, and loss evaluation. Manufacturers typically provide SPICE behavioral models to characterize the static and dynamic properties of power devices, particularly the effects of voltage-dependent junction capacitances on switching transients and energy-related metrics such as C_{oss} [16]. However, although SPICE models can be executed in circuit simulators, modeling and simulation based on Simulink/Simscape are often more convenient and efficient for system-level studies involving control algorithms and multi-domain coupling. Even when co-simulation interfaces are available, system-level design and control validation of PV DC–DC converters still tend to rely on multi-domain collaborative simulation platforms such as Simulink/Simscape, considering the overall operational complexity and simulation efficiency [17]. When SPICE subcircuits are directly migrated into Simscape, differences in modeling semantics often lead to compilation or numerical convergence problems, especially in the charge- and capacitance-based representations of voltage-dependent capacitances. In the absence of an available and reliable device model, the value of system-level simulation in predicting soft-switching conditions, evaluating switching-loss trends, and guiding device and parameter selection is significantly constrained [12].

2 BEHAVIORAL MODEL AND SIMSCAPE COMPATIBILITY ISSUES

2.1 Charge-Based Representation of Voltage-Dependent Capacitances in Behavioral Models

To accurately capture the strong nonlinearity of GaN device parasitic capacitances in transient simulations, as well as their effects on dv/dt, switching loss, and soft-switching conditions, manufacturer-provided SPICE behavioral models typically employ a charge-based formulation for nonlinear capacitances. Taking the EPC2302 as an example, the core idea is to describe the voltage-dependent characteristics of the device terminals through a charge function $q(v)$, from which the current through the capacitive branch is naturally obtained as the time derivative of charge:

$$i(t)=\frac{dq(v)}{dt}=\frac{dq}{dv}\frac{dv}{dt}=C(v)\frac{dv}{dt} \tag{1}$$

Compared with directly fitting the capacitance function $C(v)$, the charge-based formulation is more conducive to preserving energy consistency and passivity constraints, and can be directly related to capacitance-, charge-, and energy-based metrics commonly reported in device datasheets. Existing studies have established input, output, and reverse capacitance models for GaN HEMTs, including parasitic capacitances, from physical and analytical perspectives in order to explain their bias-dependent behavior [18-20]. However, such models usually rely on a large number of device structural and process parameters and involve relatively complex parameter extraction procedures. Considering both model accessibility and the convenience of engineering validation, this paper adopts the terminal-equivalent capacitances commonly provided in datasheets, namely C_{oss}, C_{iss}, and C_{rss}, as the modeling and validation targets. This choice facilitates direct correspondence with publicly available characteristic curves and supports the requirements of system-level simulation, see Figure 1. In the EPC2302 datasheet, the typical curves show the variation of terminal-equivalent capacitances with V_{ds}, and their relationships are given by:

$$\begin{cases} C_{iss}=C_{gs}+C_{gd} \\ C_{rss}=C_{gd} \\ C_{oss}=C_{gd}+C_{ds} \end{cases} \tag{2}$$

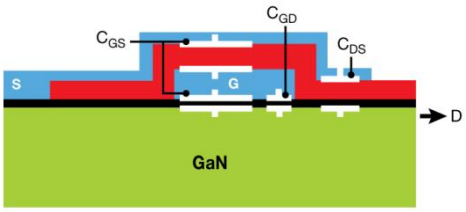

Figure 1 Schematic diagram of intrinsic capacitance distribution in a GaN HEMT

Therefore, in the device behavioral modeling developed in this paper, the terminal-equivalent capacitances observable from the datasheet are used as constraints, while charge–voltage functions are employed to characterize the nonlinear behavior of the gate–drain and drain–source branches, such as $q_{gd}(v_{gd})$ and $q_{ds}(v_{ds})$. The corresponding capacitive branch currents are then obtained from the relationship between branch current and the time rate of change of charge. In this way, the model preserves consistency with the mappings to the C_{iss}, C_{rss}, and C_{oss}curves, while also satisfying the requirements of transient simulation.

2.2 Syntactic Conflicts in the Migration from SPICE to Simscape

Although charge-based behavioral models can be implemented directly on SPICE platforms, syntactic conflicts arise when they are migrated to the Simulink/Simscape environment. SPICE allows node voltages, such as $v(a,b)$, to be directly accessed as runtime variables in charge or current expressions, thereby enabling the implementation of voltage-dependent capacitances in the form of $q(v)$ or $i(v,\dot{v})$. In Simscape, however, the parameters of fundamental components are typically determined at compile time or during initialization, and are not allowed to depend on runtime *across* variables, such as terminal voltages $V_{ds}$and V_{gs}. Therefore, when a SPICE subcircuit is mapped into a Simscape component using an automatic conversion tool, compilation may fail if the converter incorrectly represents the charge-based dynamic relationship as a form in which the component parameter varies with voltage—that is, if it attempts to define $C=f(v(t))$within a basic capacitor element. In such a case, the compiler encounters a contradiction in which a parameter is made dependent on a runtime state variable, leading to failure when the Simscape compilation command is invoked. The root cause does not lie in the mathematical form of the charge function itself, but rather in the conflict between two modeling principles: dynamic relationships must be solved explicitly at the equation level, whereas component parameters must remain static. Accordingly, charge-based nonlinear capacitances must be introduced explicitly in equation form, rather than being reduced to direct functions of basic component parameters.

2.3 Problem Summary and Reconstruction Objective

In summary, the fundamental reason why manufacturer-provided SPICE behavioral models cannot be directly used in the Simscape environment is that, during automatic conversion, the dynamic relationship of charge-based nonlinear capacitances, $i=dq(v)/dt$, is improperly mapped into a parameterized capacitance form of a basic component, namely $c=f(v)$. This causes a semantic conflict in which a compile-time parameter depends on a runtime voltage variable. To preserve the dynamic behavior equivalent to that of the original SPICE model on the Simscape platform, the voltage-dependent capacitance must be reconstructed from a *component parameter* into a *branch equation*, and implemented in the equivalent capacitance form:

$$\mathrm{i(v)=C(v)}\frac{\mathrm{dv}}{\mathrm{dt}} \tag{3}$$

Accordingly, the objective of the subsequent reconstruction in this paper is to retain the fitted structure and physical meaning of the manufacturer-defined charge function $q(v)$, while separating it from the parameterized expressions generated by automatic conversion and reformulating it into an explicit branch-equation form that is compilable in Simscape. Based on this reconstructed model, comparative validation of key device dynamic characteristics and system-level simulation of switching transients are then carried out.

3 SIMSCAPE-ORIENTED EQUIVALENT MODELING METHOD FOR VOLTAGE-DEPENDENT CAPACITANCES

3.1 Modeling Objective

GaN devices exhibit pronounced voltage-dependent parasitic capacitance characteristics during high-frequency switching, among which the nonlinearity of output-related capacitances directly affects the switching-node dv/dt, switching loss, and soft-switching conditions. Equation (2) has already described the variation of terminal-equivalent capacitances with V_{ds}. If equivalent models of $C_{gd}(v)$and $C_{ds}(v)$that vary with terminal voltage can be constructed, the key capacitance nonlinearities reflected in the datasheet curves can be reproduced in system-level simulations. Such a model can also be further used to evaluate switching-loss-related quantities, including the drain–source output charge Q_{oss} and output energy E_{oss}. Therefore, the objective of this study is to preserve the ability of the manufacturer's behavioral model to represent voltage-dependent capacitances on the Simscape platform, while simultaneously satisfying the constraints imposed by Simscape compilation and numerical solution.

3.2 Equation Implementation

As discussed previously, during the conversion of a SPICE model into a Simscape model, a voltage-dependent capacitance may be incorrectly mapped into a parasitic capacitor component parameter in the form of $C=f(v)$, thereby causing a syntactic error in which a compile-time parameter depends on a runtime voltage variable. To avoid this problem, the present study introduces the voltage-dependent capacitance as a runtime function $C(v)$ and explicitly defines, within the equations of the Simscape component, the relationship between the capacitive branch current and the time derivative of the terminal voltage. For an arbitrary voltage-dependent capacitive branch, the branch current can be expressed as:

$$i_c(t)=C\big(v(t)\big)\frac{dv(t)}{dt} \tag{4}$$

where $v(t)$ denotes the corresponding terminal-to-terminal voltage, such as v_{gd}, v_{gs}, or v_{sd}, and $i_C(t)$ is the current through the capacitive branch. This formulation is mathematically equivalent to the charge-based representation in which the branch current is obtained by differentiating charge with respect to time. Its essential advantage lies in separating the voltage-dependent relationship from the parameter definition of the fundamental component and instead introducing it into the solution process in the form of explicit equations, thereby satisfying the compilation semantics of Simscape while preserving the required dynamic characteristics.

3.3 Smooth Fitting of Voltage-Dependent Capacitance Functions

To characterize capacitance nonlinearity over the full voltage range while ensuring numerical stability in the solution process, manufacturer-provided behavioral models typically employ smooth functions to fit piecewise characteristics. Following this modeling concept, this paper represents the voltage-dependent capacitance as a superposition of several smooth basis functions:

$$C(v)=C_0+\sum_{k=1}^{N} a_k\phi\left(\frac{v\text{-}V_k}{s_k}\right) \tag{5}$$

where $C_0$is a constant term, a_k, V_k, and $s_k$are fitting coefficients and scaling parameters, and ϕdenotes a continuously differentiable smooth basis function. The purpose of adopting such a representation is that it avoids hard transition

points between different operating regions, thereby effectively reducing numerical oscillations and convergence risks of the implicit solver under high- dv/dt conditions. Based on this formulation, the present study implements the corresponding branch current at the Simscape equation level as $i_C=C(v)\,dv/dt$, thereby enabling both the applicability and numerical stability of voltage-dependent capacitance modeling in system-level transient simulations.

3.4 Model Conversion and Integration Procedure

After completing the above equivalent modeling and mathematical reformulation, the manufacturer-provided SPICE subcircuit netlist is taken as the input in this study. First, the MATLAB built-in function subcircuit2ssc is used to convert the netlist into a Simscape .ssc component description file. Subsequently, the portions of the converted result that are incompatible with Simscape syntax are manually modified and reconstructed. Finally, the revised model is compiled into a reusable Simscape electrical device module. This module provides a unified modeling basis for the subsequent comparison of key device characteristics and the system-level transient validation.

4 MODEL VALIDATION AND EFFECTIVENESS EVALUATION

4.1 Validation Strategy and Test Platform

To verify the effectiveness of the reconstructed Simscape device model in system-level simulations, a three-level validation strategy is adopted in this study, consisting of static conduction characteristics, nonlinear capacitance characteristics, and charge/energy-related metrics. At the static level, the on-state behavior of the device under given gate-voltage and current conditions is aligned through $R_{\mathrm{ds(on)}}$. At the capacitance level, directly observable datasheet quantities are used as the reference, with particular emphasis on matching the variation trends of C_{iss}, C_{rss}, and C_{oss} with V_{DS}, based on the EPC2302 datasheet curves [21]. On this basis, the output charge Q_{oss} and output energy E_{oss}, which are determined by the nonlinear capacitances, are further extracted and evaluated in order to validate the model consistency at the charge and energy scales.

4.2 Validation of Static Conduction Characteristics

To evaluate the capability of the model to represent device characteristics related to conduction loss, the on-state resistance $R_{\mathrm{ds(on)}}$ is extracted under quasi-static conditions and compared with the typical values specified in the datasheet under corresponding test conditions. In the on-state, the device current I_D is fixed, while the gate-to-source voltage V_{gs} is varied slowly, and the corresponding $R_{\mathrm{ds(on)}}$ values are recorded. The calculation is given by:

$$R_{ds(on)}=\frac{V_{ds}}{I_D} \tag{6}$$

This result is used to verify whether the equivalent resistance parameterization of the model in the conduction region is consistent with the datasheet, and also provides a basis for subsequent system-level efficiency and loss analysis, see Figure 2.

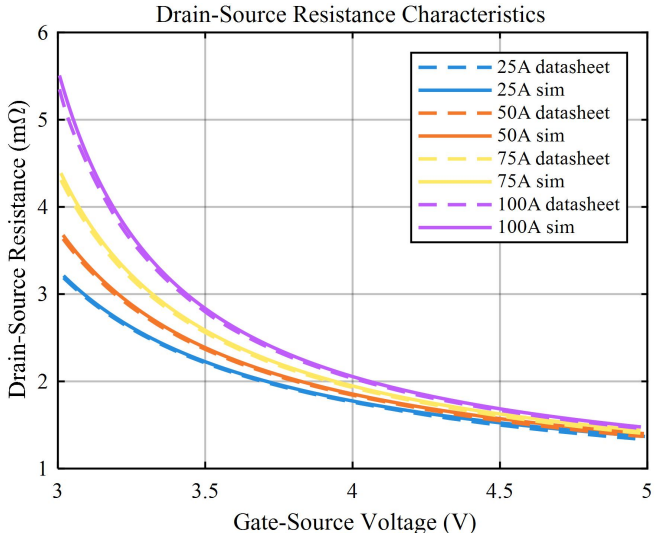

Figure 2 Comparison of $R_{ds(on)}$-V_{gs} Characteristics under Different Current Conditions

4.3 Validation of Voltage-Dependent Capacitance Curves

Using the typical curves provided in the EPC2302 datasheet as the reference, this study performs quasi-static bias

sweeps on the device in the Simscape platform. The terminal-equivalent capacitances at different V_{ds} values are extracted using a small-signal AC excitation under DC bias sweep [22, 23]. By injecting a small AC voltage and measuring the resulting AC current, the incremental capacitance can be obtained from the admittance relationship. The primary focus is on whether the overall variation trends of the junction capacitances with respect to V_{ds} are consistent, and quantitative errors are further reported over the voltage range of 10–48 V, see Figure 3.

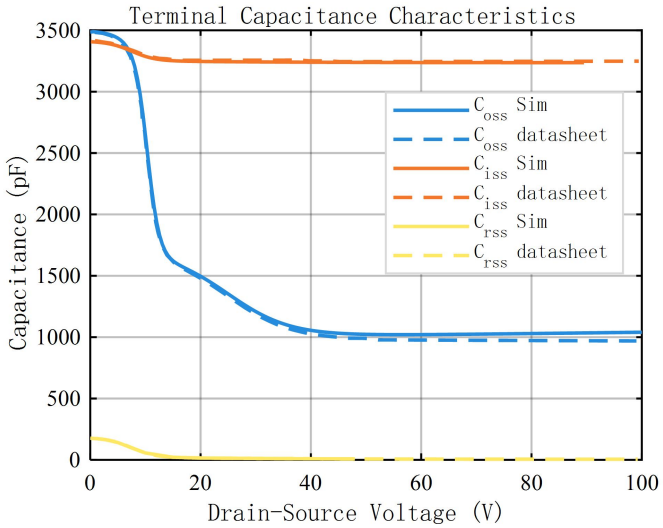

Figure 3 Comparison of Equivalent Terminal Capacitance (C–V) Characteristics

4.4 Validation of Charge/Energy Metrics (Q_{oss} and E_{oss})

To further verify the consistency of the nonlinear capacitance model on the energy scale, Q_{oss} and E_{oss} are derived from the charge–voltage characteristics of the device. The corresponding quantities are obtained by integrating the nonlinear capacitance over the drain voltage range [24, 25]. In the Simscape model, a controlled excitation is applied to the output terminal, and the corresponding $v(t)$ and $i(t)$ are recorded. The quantities are then calculated as:

$$\begin{cases} &Q_{oss}(v)=\int i(t)dt \\ &E_{oss}(v)=\int v(t)i(t)dt \end{cases} \tag{7}$$

The extracted results are then compared for consistency with the typical values provided in the datasheet, if available, or with reference values obtained by integrating the datasheet $C_{oss}(v)$ curve. This step extends the validation from capacitance-curve matching to charge- and energy-scale matching, thereby providing a more direct basis for switching-loss analysis, see Figure 4.

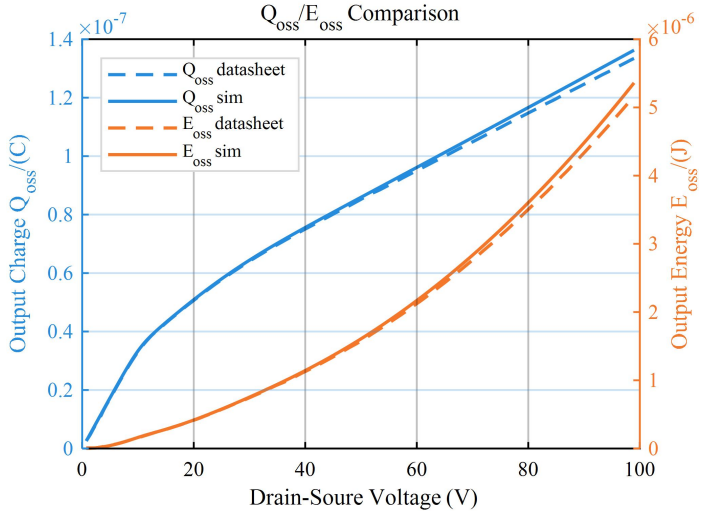

Figure 4 Comparison of Output Charge (Q_{oss}) and Output Energy (E_{oss}) versus Drain–Source Voltage

4.5 Comparison Results and Conclusion

Based on the above comparisons of static conduction characteristics and nonlinear-capacitance-related metrics, the reconstructed Simscape device model developed in this study is able to maintain consistency with the datasheet

references in terms of key electrical characteristics. The maximum relative error between the extracted $R_{ds(on)}$ values and the typical datasheet values under different conduction-current conditions is 3.29%. The terminal-equivalent capacitance curves, namely C_{iss}, C_{rss}, and C_{oss}, exhibit overall variation trends consistent with the datasheet over the V_{ds} range of 0–100 V, with an average error of less than 4%. In addition, the deviations of Q_{oss} and E_{oss}, obtained through transient integration, are both within 3% relative to the reference values. A summary of these metrics and errors is provided in Table 1.

Table 1 Error Summary of Aligned Key Electrical Characteristics

Parameter	RMSE	MAPE	Maximum Relative Error	R^2
C_{iss}	$10.32pF$	0.31%	0.505%	0.93
C_{oss}	$42.25pF$	3.62%	7.26%	0.99
C_{rss}	$0.69pF$	1.04%	6.08%	0.99
Q_{oss}	$1.3nF$	1.2%	5.77%	0.99
E_{oss}	$74.21nJ$	2.98%	8.99%	0.99

These results indicate that, after reformulating the voltage-dependent capacitances from parameterized expressions into equation-level branch-current representations, the model not only preserves the fitting structure of the manufacturer-provided behavioral model, but also achieves compilable and convergent capability for system-level simulation. It can therefore be used for subsequent analysis of switching transients and loss trends at the converter-topology level. The remaining discrepancies may arise from factors such as differences between the simulation conditions and the datasheet test conditions. Accordingly, the proposed model is more suitable for trend evaluation, efficiency analysis, and parameter-sensitivity studies, rather than for replacing full-parasitic models in precise waveform prediction.

COMPETING INTERESTS

The authors have no relevant financial or non-financial interests to disclose.

REFERENCES

[1] Yao Yubi, Zheng Shaozhong, Yang Yang, et al. Progress and prospects of solar energy resource assessment and utilization efficiency in China. Acta Energiae Solaris Sinica, 2022, 43(10): 524-535.
[2] Xia Ziyi, Ji Haichen, Kong Jiake, et al. Design of a time-division multiplexing-based photovoltaic DMPPT system. Acta Energiae Solaris Sinica, 2025, 46(12): 288-297.
[3] Zhong Qida. Research on a bidirectional DC/DC converter and its control strategy for photovoltaic energy storage. Liuzhou: Guangxi University of Science and Technology, 2024. DOI: 10.27759/d.cnki.ggxgx.2024.000600.
[4] Qiu Zhaochuan. Research on parallel current sharing and high-frequency transformer of a photovoltaic DC collection clamped resonant DC/DC converter. Harbin: Harbin Institute of Technology, 2025. DOI: 10.27061/d.cnki.ghgdu.2025.003374.
[5] Lidow A D R M, Strydom J, et al. GaN transistors for efficient power conversion. WILEY, 2019.
[6] Xu Wenzhe. Research on a GaN-based series-resonant high-frequency-link photovoltaic microinverter. Wuhan: Huazhong University of Science and Technology, 2024. DOI: 10.27157/d.cnki.ghzku.2024.002179.
[7] Zheng Kefang. Research on a single-phase photovoltaic inverter based on gallium nitride devices. Xuzhou: China University of Mining and Technology, 2025. DOI: 10.27623/d.cnki.gzkyu.2025.000323.
[8] L Garcia-Rodriguez, V Jones, JC Balda, et al. Design of a GaN-based microinverter for photovoltaic systems. 2014 IEEE 5th International Symposium on Power Electronics for Distributed Generation Systems (PEDG), Galway, Ireland. 2014, 1-6. DOI: 10.1109/PEDG.2014.6878639.
[9] Karimzada O, Donato G D. Design and Verification of a GaN-Based, Single Stage, Grid-Connected Three-Phase PV Inverter. IEEE Transactions on Power Electronics, 2025, 40(4): 5496-5504. DOI: 10.1109/TPEL.2024.3511270.
[10] Stubbe T, Mallwitz R, Rupp R, et al. GaN power semiconductors for PV inverter applications-Opportunities and risks. Proceedings of the CIPS 2014; 8th International Conference on Integrated Power Electronics Systems, Nuremberg/German, 2014 of Conference: VDE, 2014, 1-6.
[11] Du C, Ye R, Cai X, et al. A review on GaN HEMTs: nonlinear mechanisms and improvement methods. Journal of Semiconductors, 2023, 44(12). DOI: 10.1088/1674-4926/44/12/121801.
[12] Matthias Kasper, Dominik Bortis, Johann W Kolar. Classification and Comparative Evaluation of PV Panel-Integrated DC–DC Converter Concepts. IEEE Transactions on Power Electronics, 2014, 29(5): 2511-2526. DOI: 10.1109/TPEL.2013.2273399.
[13] Raghavendra K V G, Zeb K, Muthusamy A, et al. A Comprehensive Review of DC–DC Converter Topologies and Modulation Strategies with Recent Advances in Solar Photovoltaic Systems. Electronics 2020, 9(1): 31.
[14] Omar Abdel-Rahim, Andrii Chub, Dmitri Vinnikov, et al. DC Integration of Residential Photovoltaic Systems: A Survey. IEEE Access, 2022, 10, 66974-66991. DOI: 10.1109/ACCESS.2022.3185788.

[15] Choi WY, Lee CG. Photovoltaic panel integrated power conditioning system using a high efficiency step-up DC–DC converter. Renewable Energy, 2012, 41, 227-234. DOI: 10.1016/j.renene.2011.10.023.
[16] Wang Kangping, Tian Mofan, Li Hongchang, et al. An improved switching loss model for a 650V enhancement-mode GaN transistor. 2016 IEEE 2nd Annual Southern Power Electronics Conference (SPEC), Auckland, New Zealand. 2016, 1-6. DOI: 10.1109/SPEC.2016.7846144.
[17] Cao Haiyang, Li Bo, Chen Feiyang, et al. Voltage oscillation testing of gallium nitride switching devices based on Simulink. Experiment Technology and Management, 2025, 42(10): 130-136.
[18] Čučak D, Vasić M, García O, et al. Physics-Based Analytical Model for Input, Output, and Reverse Capacitance of a GaN HEMT With the Field-Plate Structure. IEEE Transactions on Power Electronics, 2017, 32(3): 2189-2202.
[19] Zhang Aixi, Zhang Lining, Tang Zhikai, et al. Analytical Modeling of Capacitances for GaN HEMTs, Including Parasitic Components. IEEE Transactions on Electron Devices, 2014, 61(3): 755-761.
[20] Jia Yonghao, Xu Yuehang, Wen Zhang, et al. Analytical Gate Capacitance Models for Large-Signal Compact Model of AlGaN/GaN HEMTs. IEEE Transactions on Electron Devices, 2019, 66(1): 357-363.
[21] Corporation E P C. EPC2302 – Enhancement Mode Power Transistor: eGaN® FET Datasheet: Efficient Power Conversion Corporation, 2025.
[22] Cho T, Park J, Jung S, et al. Analysis and Modeling of Intrinsic Capacitance in Enhancement Mode GaN HEMT. IEEE Journal of the Electron Devices Society, 2025, 13, 638-641.
[23] Samizadeh Nikoo M, Jafari A, Perera N, et al. Measurement of Large-Signal COSS and COSS Losses of Transistors Based on Nonlinear Resonance. IEEE Transactions on Power Electronics, 2020, 35(3): 2242-2246.
[24] Huang Y, Jiang Q, Huang S, et al. In-Situ Extraction of Time-Resolved Eoss on GaN Power Device Based on a Modified Hard Switching Platform. 2024 36th International Symposium on Power Semiconductor Devices and ICs (ISPSD), Bremen, Germany, 2024, 259-262. DOI: 10.1109/ISPSD59661.2024.10579648.
[25] Hou R, Lu J, Chen D. Parasitic capacitance Eqoss loss mechanism, calculation, and measurement in hard-switching for GaN HEMTs. 2018 IEEE Applied Power Electronics Conference and Exposition (APEC), San Antonio, TX, USA. 2018, 919-924. DOI: 10.1109/APEC.2018.8341124.